AIMS Mathematics, 9(3): 6603–6627.
DOI: 10.3934/math.2024322
Received: 22 December 2023
Revised: 13 January 2024
Accepted: 26 January 2024
Published: 06 February 2024

http://www.aimspress.com/journal/Math

Research article

An optimal power flow solution for a power system integrated with renewable generation

Hisham Alghamdi[1], Lyu-Guang Hua[2], Muhammad Riaz[3], Ghulam Hafeez[4,*], Safeer Ullah[5], Monji Mohamed Zaidi[6], and Mohammed Jalalah[1,*]

[1] Electrical Engineering Department, College of Engineering, Najran University, Najran 11001, Saudi Arabia; Email: hg@nu.edu.sa, jalalah@gmail.com
[2] Power China Hua Dong Engineering Corporation Limited, Hangzhou 311122, China Hangzhou 311122, China; Email: lv_gh@hdec.com
[3] Khyber Pakhtunkhwa Technical Education & Vocational Training Authority, Peshawar, Pakistan; Email: mriaz385@gmail.com
[4] Department of Electrical Engineering, University of Engineering and Technology, Mardan 23200, Pakistan; Email: ghulamhafeez393@gmail.com
[5] Department of Electrical Engineering, Quaid-e-Azam College of Engineering & Technology, Sahiwal, 57000, Pakistan; Email: safeer_iiui@yahoo.com
[6] Department of Electrical Engineering-College of Engineering-King Khalid University-Abha-Saudi Arabia; Email: amzaydi@kku.edu.sa

* **Correspondence:** Email: ghulamhafeez393@gmail.com, jalalah@gmail.com.

Abstract: Integrating Green Renewable Energy Sources (GRES) as substitutes for fossil fuel-based energy sources is essential for reducing harmful emissions. The GRES are intermittent and their integration into the conventional IEEE 30 bus configuration increases the complexity and nonlinearity of the system. The Grey Wolf optimizer (GWO) has excellent exploration capability but needs exploitation capability to enhance its convergence speed. Adding particle swarm optimization (PSO) with excellent convergence capability to GWO leads to the development of a novel algorithm, namely a Grey Wolf particle swarm optimization (GWPSO) algorithm with excellent exploration and exploitation capabilities. This study utilizes the advantages of the GWPSO algorithm to solve the optimal power flow (OPF) problem for adaptive IEEE 30 bus systems, including thermal, solar photovoltaic (SP), wind turbine (WT), and small hydropower (SHP) sources. Weibull, Lognormal, and Gumbel probability density functions (PDFs) are employed to forecast the output power of WT, SP,

and SHP power sources after evaluating 8000 Monte Carlo possibilities, respectively. The multi-objective green economic optimal solution consisted of 11 control variables to reduce the cost, power losses, and harmful emissions. The proposed method to address the OPF problem is validated using an adaptive IEEE bus system. The proposed GWPSO algorithm is evaluated by comparing it with PSO and GWO optimization algorithms in terms of achieving an optimal green economic solution for the adaptive IEEE 30 bus system. This evaluation is conducted within the confines of the same test system using identical system constraints and control variables. The integration of a small SHP with WT and SP sources, along with the proposed GWPSO algorithm, led to a yearly cost reduction ranging from **$19,368** to **$30,081**. Simulation findings endorsed that the proposed GWPSO algorithm executes fruitfully compared to alternative algorithms regarding a consistent convergence curve and robustness, proving its potential as a viable choice for achieving cost-effective solutions in power systems incorporating GRES.

Keywords: power system; green distributed generation; photovoltaic; wind; hydropower; optimal power flow
Mathematics Subject Classification: 68T20

1. Introduction

The intensifying demand for several industries has led the world to a concerning upsurge in the production of injurious gases, which openly damage the environment. This mounting demand is mostly driven by population increase, development, and user needs, putting tension on energy resources. To deal with the huge demand for energy, the energy production sector and other industries are releasing greenhouse gases and other toxins into the atmosphere, escalating worldwide environmental issues such as climate change and air pollution.

The energy production sector and industries deeply depend on fossil fuels, like petroleum, methane, and coal, utilized for generating energy and manufacturing processes. The energy produced through the burning of fossil fuels leads to the emission of substantial quantities of carbon dioxide (CO_2), which is accountable for trapping heat in the atmosphere, triggering global warming. The drastic changes in climate change, the significant increase in energy demand and an upsurge in fossil fuel prices compel the world on the road to the addition of green renewable energy sources (GRES) along with fossil fuel-based conventional sources [1]. The incorporation of solar, wind, and hydropower sources into energy systems is a transformative strategy that aligns industrial growth with environmental stewardship [2]. The study explores the impact of clean energy and carbon markets on environmental sustainability, investigating interdependencies and spillover effects between global carbon and GRES like wind, solar, biofuel and geothermal [3]. This approach not only caters to the escalating energy requirements but also paves the way for a cleaner, more sustainable future, fostering a harmonious coexistence between industrial progress and ecological preservation [4]. Optimal Power Flow (OPF) emerges as a pivotal optimization challenge within power systems, seeking to minimize generation expenses while upholding operational limitations. With the rising integration of GRES like wind, solar, and hydropower sources, the complication and non-linearity of the OPF problem further intensify [5]. However, to address this intermittent and fluctuating nature of GRES, batteries are required [6].

Over the past few years, numerous optimization algorithms and approaches have been created and applied to address the optimization challenges associated with the OPF problem. These include traditional techniques, evolutionary strategies, and sophisticated metaheuristic algorithms. Linear programming (LP) is a conventional method applied to solve OPF problems, as cited in [7]. Non-linear programming (NLP) technique presented in [8] has been employed for addressing OPF problems. Quadratic programming (QP) has been utilized in solving OPF problems by the researchers in [9]. Dynamic programming (DP) represented in [10] is another traditional approach applied to address OPF problems. The interior point (IP) method, as outlined in [11], has been employed in tackling of OPF problems. Nevertheless, these classical approaches encounter limitations when dealing with large-scale problems due to their complex and intensive computations, as well as their prominent reliance on initial estimation values. Algorithms derived from the principles of evolution mimic the evolutionary process, generating successive generations through mating to achieve optimal solutions. The authors in [12] have utilized the genetic optimization algorithm (GOA) to tackle the OPF in distribution systems. Enhanced genetic algorithm (GA) has been used in [13] for the solution of multi objective OPF problem. Another notable contender in this category is the Differential Evolution (DE) algorithm, which has demonstrated efficacy in handling constraints while optimizing diverse objectives within the OPF context [14]. In order to prevail over the limitations of conventional and evolutionary-driven approaches, a number of heuristic algorithms were adeptly employed to address the OPF challenge. Particle swarm optimization (PSO), as cited in [15], stands out as a prominently used metaheuristic algorithm for solving OPF problems. Moth-flame optimization (MFO) algorithm discussed in [16], is another metaheuristic algorithm widely employed in the context of OPF solution. The multi-verse optimization (MVO) algorithm, as introduced in [17], is recognized as a prominent metaheuristic approach for addressing OPF challenges. Moth-swarm algorithm (MSA), described in [18], is among the widely used metaheuristic algorithms in the field of OPF solution. The elephant herding algorithm (EHA), outlined in [19], is acknowledged as a notable metaheuristic approach for optimizing OPF problems. Gravitational search algorithm (GSA), detailed in [20], is recognized as a key metaheuristic algorithm applied in the resolution of OPF issues. The whale optimization algorithm (WOA), discussed in [21], is a notable metaheuristic approach frequently utilized for solving OPF problems. Grey wolf optimization (GWO), highlighted in [22], is a metaheuristic algorithm extensively used in the domain of OPF solution. The ant lion algorithm (ALA), introduced in [23], is recognized as a significant metaheuristic approach for OPF optimization. The grasshopper algorithm (GA), as cited in [24], is recognized as a noteworthy metaheuristic algorithm employed for OPF solution.

In the struggle of enhancing the global search competences of metaheuristic algorithms, the combination of two algorithms has been undertaken to attain globally optimal results. One of the algorithms used for OPF is the fusion of dragonfly and PSO (DA-PSO), as proposed in reference [25]. This hybridization of both algorithms harnesses the strengths of both, augmenting their abilities in both exploitation and exploration. The efficacy of the selected DA-PSO algorithm has been substantiated through testing on systems involving IEEE 30 and 57 buses, encompassing various objective functions. PSO-GSA, as referenced in [26], is an optimization algorithm distinctively applied to address OPF problems. Harris hawk optimization combined with DE (HHODE), introduced in [27], represents an innovative approach for OPF optimization. Hybridizing cuckoo search with GWO (HCSGWO), detailed in [28], is a unique optimization algorithm employed in solving OPF challenges. The combination of cross entropy with CSA (CE-CSA), as discussed in [29], offers a novel strategy for addressing OPF optimization concerns. A hybrid PSO-GWO algorithm has been employed in [30], to

address the OPF problem for IEEE modified 30-bus systems including solar and wind energy sources. The researchers in [31] employed the enhanced computational optimizer of the social network search technique (ESNST) to find multidimensional OPF solutions for IEEE-30, 57, and 118 bus systems, without taking into account the integration of GRES. The gorilla troops optimization technique (GTOT), inspired by the collective behaviors of gorilla groups, has been successfully applied to optimize fuel costs, emissions, and power losses in IEEE-30 bus systems [32].

The IEEE 30 bus system is a well-known benchmark system employed for assessing the usefulness of optimization algorithms in power systems. This study proposes a GWPSO algorithm to alleviate generation costs, power losses and pollution emissions for a system integrated with GRES such as wind turbine (WT), solar photovoltaic (SP) and small hydropower (SHP) sources. The GWPSO algorithm merges the exploration competence of the GWO algorithm with the exploitation competence of the PSO algorithm. The usefulness and proficiency of the proposed algorithm are assessed by comparing it with other optimization techniques such as PSO and GWO. This work is a continuation of the earlier works [5,30], where OPF problem is solved for IEEE modified 30 bus systems integrated with solar and wind energy sources using HPS-GWO and PSO-GWO algorithms, respectively. Validation is endorsed via comparison with SHADE-SF, GWO, and PSO.

The rest of the paper is organized as follows. Section 2 presents the OPF formulation for IEEE 30 bus system integrated with WT, SP and SHP sources. Section 3 describes the uncertainty modeling and probability density functions (PDFs) for WT, SP and SHP sources. Section 4 presents the proposed GWPSO algorithm. Section 5 provides details of the simulation outcomes and analysis. Finally, in Section 6 the paper concludes by providing a concise over-view of the findings and offering suggestions for potential avenues of future research.

2. Formulation OPF and determination of cost functions

The methodology involves the formulation of OPF with GRES, formulation of the Objective/Cost Function, modeling the uncertainty of GRES, hybridization of the GWO with PSO algorithm, setting initialization and termination criteria, and conducting performance evaluation and result validations. The IEEE 30-bus system in its standard form comprises twenty-four buses for load distribution and six buses for generators, where thermal generators (TGs) are linked. In the suggested altered system, three TGs have been substituted with two WTs sources (at buses 5 and 11) and a SP source combined with a SHP source (at bus 13). This replacement aims to formulate an OPF as an optimization challenge characterized by both inequality and equality constraints to reduce emissions and generation costs [30]. The essentials of the system being examined, as outlined in Table 1, include TGs, WTs and SP combined with SHP sources. Moreover, Figure 1 illustrates the composition of the test system under study.

Table 1. Adopted modified IEEE 30 bus system details.

Parameters	Quantity	Details
Buses	30	[5]
Branches	41	[5]
TGs	3	at bus# 1, 2 and 8 (bus 1: swing)
WTs	2	at bus# 5 and 11
SP	1	at bus# 13
SHP	1	at bus# 13
Load connected	-	P=283.4 MW, Q=126.3 MVAr
Shunt compensators	2	Q=0.19MVAr at bus 5 and Q=0.04 MVAr at bus 24
Load buses voltage (p.u.)	24	[0.95-1.05]
Generation buses voltage (p.u.)	6	[0.95-1.10]
Controlling parameters	11	Real power (MW) for all generation buses except slack and voltages (p.u.) for all generation buses

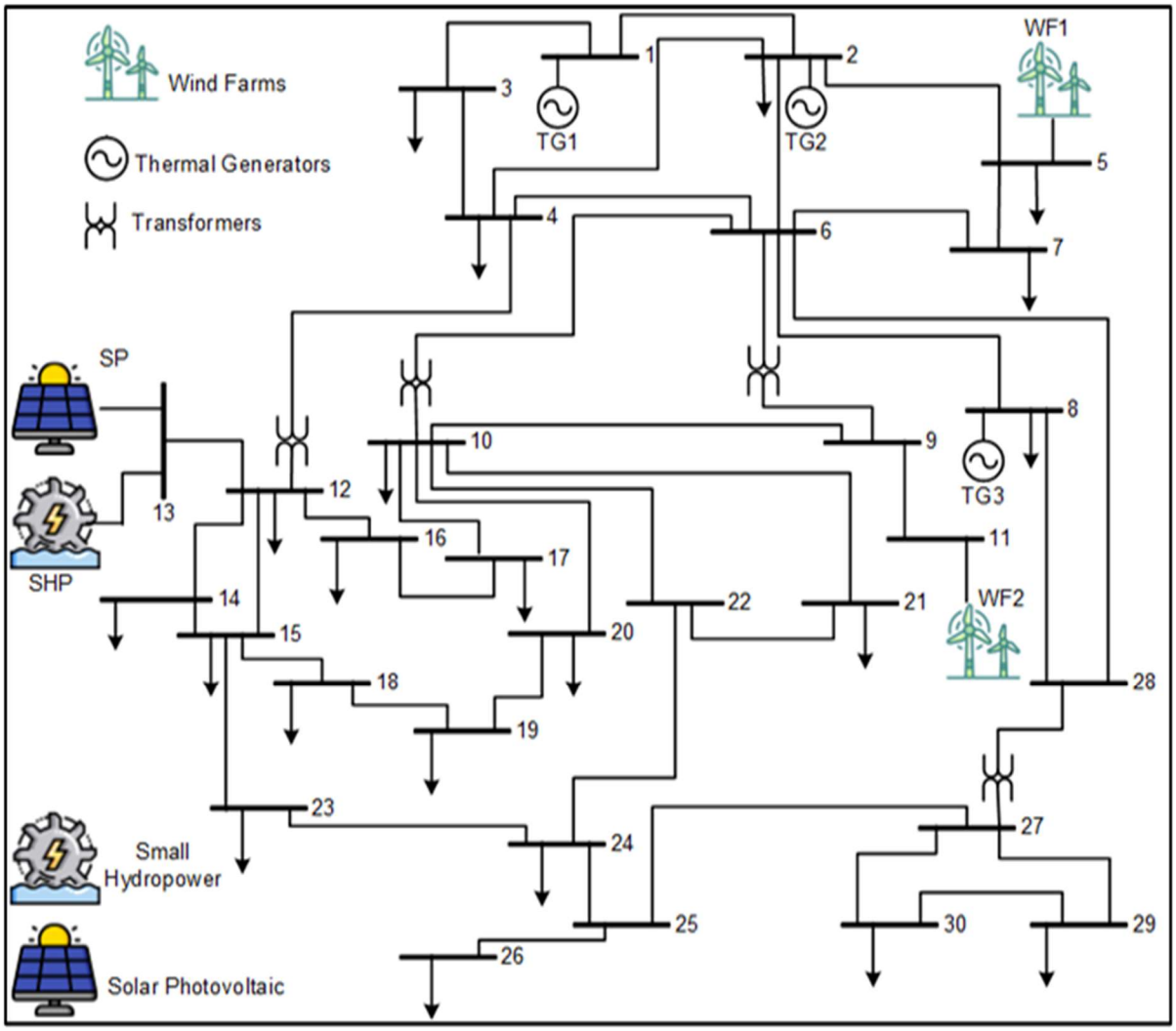

Figure 1. An adaptive IEEE 30 bus system employed for OPF evaluation.

2.1 The cost functions for thermal generators (TGs)

The detailed mathematical modeling of the system can be found in [5], where two WT and a SP source are connected. The output power of TG relies on fossil fuels. The correlation between the produced power (MW) and the cost of fuel ($/hr) can be determined using the subsequent quadratic equation:

$$C_{TG} = \sum_{i=1}^{nT} a_i + b_i + c_i P_{TGi}^2 . \tag{1}$$

C_{TG} denotes the overall cost where the parameters a_i, b_i, and c_i signify the fuel cost coefficients for the i^{th} TGs, and their specific values are detailed in Table 2.

Table 2. The numerical values of cost and emission coefficients for TGs used in Eqs (1)–(4).

TG at Bus #	$P_{TGi}^{\min}(MW)$	$P_{TGi}^{\max}(MW)$	a	b	c	d	e	α	β	γ	ω	μ^T
1	50	200	0	2	0.00375	18	0.037	4.091	−5.554	6.49	6.667	0.0002
2	20	80	0	1.75	0.0175	16	0.038	2.543	−6.047	5.638	3.333	0.0005
8	10	35	0	3.25	0.00834	12	0.045	5.326	−3.55	3.38	2	0.002

For accurate modeling of the cost function for TGs, the valve point effect needs to be considered.

$$C_{TG-V} = \sum_{i=1}^{nT} a_i + b_i + c_i P_{TGi}^2 + \left| d_i \times \sin\left\{ e_i \times \left(P_{TGi}^{\min} - P_{TGi} \right) \right\} \right| . \tag{2}$$

In Eq (2) e_i and d_i denote the valve point effect coefficients of steam turbines.

The amount of emission (ton) released from each TG is computed through Eq (3).

$$E_{em} = \sum_{i=1}^{nT} \left[\left(\alpha_i + \beta_i P_{TGi} + \gamma_i P_{TGi}^2 \right) \times 0.01 + \omega_i e^{(\mu^T{}_i P_{TGi})} \right] . \tag{3}$$

The emission coefficient ω_i and μ^T specific values are provided in Table 2.

In order to diminish the release of detrimental emissions and promote the incorporation of eco-friendly and economically viable GRES like SP, WT, and SHP sources, a carbon tax is implemented based on the amount of emissions produced per unit [33]. The cost associated with emissions ($/hr) for TGs is outlined as follows [5]:

$$C_{em} = C_t \times E_{em} . \tag{4}$$

The numerical values of cost and emission coefficients for TGs employed in Eqs (1)–(4) are provided in Table 2 and these values are in accordance with reference [5].

2.2 The cost functions for wind turbines (WTs) sources

Unlike TGs, GRES do not involve any ongoing costs of fossil fuel, as they do not need fossil fuel for power generation, a price per unit production may be assigned for considering the initial investment compensation, renovation and maintenance costs to GRES. The direct, reserve (due to overestimation) and penalty (due to underestimation) costs linked with each WT source, are formulated as follows [5]:

$$C_{w,j}=g_{w,j}\times P_{w-sch,j} \tag{5}$$

$$\begin{aligned} \mathrm{C_{Rw,j}} &= K_{Rw,j}(P_{wsch,j}-P_{wac,j}) \\ &= K_{Rw,j}\int_0^{P_{wsch,j}}(P_{wsch,j}-P_{wac,j})f(p_{w,j})dp_{w,j} \end{aligned} \tag{6}$$

$$\begin{aligned} \mathrm{C_{Pw,j}} &= K_{Pw,j}(P_{wac,j}-P_{wsch,j}) \\ &= K_{Pw,j}\int_{P_{wsch,j}}^{\mathrm{P_{wr,j}}}(P_{w,j}-P_{wsch,j})f_w(p_{w,j})dp_{w,j} \end{aligned}. \tag{7}$$

Equations (5)–(7), $P_{w-sch,j}$ depicts the scheduled output power and $P_{wac,j}$ denotes the actual output power from j^{th} WT source. The $g_{w,j}$, $K_{Rw,j}$, and $K_{Pw,j}$ represents direct, reserve and penalty cost coefficient of j^{th} WT sources, respectively, there numerical values are mentioned in Table 3.

Table 3. Numerical values of cost coefficients and pdf parameters for WTs.

Bus No.	**Wind Farm No.**	P_{rw} (MW)	**Direct cost Coefficient** (g_w)	**Reserve cost Coefficient** (K_{Rw})	**Penalty cost coefficient** (K_{Pw})	**Scale factor** (c)	**Shape factor** (k)
5	1	75	1.6	3	1.5	9	2
11	2	60	1.75	3	1.5	10	2

The entire cost of WT sources is computed as:

$$\mathrm{C}_{t-WT}=\sum_{j=1}^{N_w}C_{w,j}+C_{Rw,j}+C_{Pw,j}\ . \tag{8}$$

2.3 The cost functions for solar photovoltaic (SP) and small hydropower (SHP) sources

This work is using a SP and a SHP source as the third GRES. The SHP source output contributes to a small proportion of the total system capacity [34]. As a result, it is combined with the SP source at bus 13 and is supposed to be owned by a sole private operator. The direct, reserve (due to overestimation) and penalty (due to underestimation) of the combined SP and SHP sources are calculated using the subsequent equations, respectively.

$$C_{D-sh,k}=(h_k\times P_{s-sch,k})+(h_l\times P_{hp-sch,k})=h_{d-sh}(P_{s-sch,k}+P_{hp-sch,k}) \tag{9}$$

$$\begin{aligned} \mathrm{C}_{\text{R-sh,k}} &= K_{R-sh,k}(P_{sh-sch,k} - P_{sh-ac,k}) \\ &= K_{R-sh,k} * f_{sh}(P_{sh-ac,k} < P_{sh-sch,k}) * [P_{sh-sch,k} - E(P_{sh-ac,k} < P_{sh-sch,k})] \end{aligned} \tag{10}$$

$$\begin{aligned} \mathrm{C}_{\text{P-sh,k}} &= K_{P-sh,k}(P_{sh-ac,k} - P_{sh-sch,k}) \\ &= K_{P-sh,k} * f_{sh}(P_{sh-ac,k} > P_{sh-sch,k}) * [E(P_{sh-ac,k} > P_{sh-sch,k}) - P_{sh-sch,k}] \end{aligned} \tag{11}$$

In Eq (9), $P_{s-sch,k}$, $P_{hp-sch,k}$, h_k, and h_l depicts the scheduled power and the coefficients for direct costs of SP and SHP sources, respectively. K_{R-sh} and K_{P-sh} represents the coefficients for reserve and penalty costs relating to k^{th} combined SP and SHP sources, respectively. $P_{sh-sch,k}$ and $P_{sh-ac,k}$ represent scheduled and actual available output power from combined SP and SHP source, respectively. The total cost of the combined SP and SHP source is calculated as follows:

$$\mathrm{C}_{t-sh} = \sum_{k=1}^{N_s} [C_{D-sh,k} + C_{R-sh,k} + C_{P-sh,k}]. \tag{12}$$

2.4 The Formulation of main objective function for optimization

In this research work, three objective functions have been formulated to optimize the overall generation cost. The first objective function is modeled to calculate overall generation cost, disregarding the valve point effect of TGs. It is expressed as follows:

$$\mathrm{F}_{obj-1} = C_{TG} + C_{t-WT} + C_{t-sh}. \tag{13}$$

The second objective function considers the valve point effect of TGs and is formulated for the total generation cost as follows:

$$\mathrm{F}_{obj-2} = C_{TG-V} + C_{t-WT} + C_{t-sh}. \tag{14}$$

The third objective function considers a carbon tax (20$/ton) on emissions from TGs and is formulated as follows:

$$\mathrm{F}_{obj-2} = C_{TG-V} + C_{t-WT} + C_{t-sh} + C_{emi}. \tag{15}$$

In Eqs (13)–(15), the individual cost of each source, C_{TG}, C_{TG-V}, C_{emi}, C_{t-WT} and C_{t-sh} are calculated using Eqs (1), (2), (4), (8) and (12), respectively.

Several equality, inequality, and security constraints are present, with their modeling details and mathematical equations as presented in [5,30]. The power loss (MW) and voltage deviation (p.u.) are the two other important parameters that can be calculated using the subsequent equations.

$$P_{loss} = \sum_{i=1}^{nl} \sum_{j \neq 1}^{nl} G_{ij} V_i^2 + V_j^2 - 2V_i V_j \cos(\delta_{ij}) \tag{16}$$

$$VD = \sum_{p=1}^{nl} \left| 1 - V_{lp} \right|. \tag{17}$$

The $\delta_{ij} = \delta_i - \delta_j$ represents the voltage angle difference between two buses, G_{ij} denotes transfer conductance, and nl signifies the overall count of lines within the network.

3. The formulation of stochastic power of green renewable energy sources

The output power of GRES is of stochastic nature due to their dependency on weather conditions, which are characteristically variable and indeterminate. The output power of GRES is altered by factors like haze, temperature, wind speed and river flow rate. To formulate the stochastic power output of GRES, it is necessary to consider probabilistic models that illustrate the inconsistency and unpredictability linked to their power output.

a) The formulation of stochastic power of wind turbine (WT) sources

The wind speed distribution exhibits a similar distribution like Weibull PDF and is mostly employed for modeling wind speed distribution [5]. Utilizing a Weibull PDF characterized by a shape factor (k) and a scale factor (c), the probability of wind speed $f_v(w)$ (m/s) as a function of wind speed (v) can be derive using the subsequent expression:

$$f_v(w) = \left(\frac{k}{c}\right)\left(\frac{v}{c}\right)^{k-1} e^{(-v/c)^k} \quad \text{for } 0 < v < \infty. \tag{18}$$

The values of shape (k) and scale (c) parameters have been extracted from the references [5] and are provided in Table 3. Figures 2 and 3 showcase the Weibull fitted curve and frequency distribution curves for wind speed of WTs sources at bus 5 and 11, respectively. These graphs are generated through the execution of 8000 Monte Carlo scenarios in the simulation.

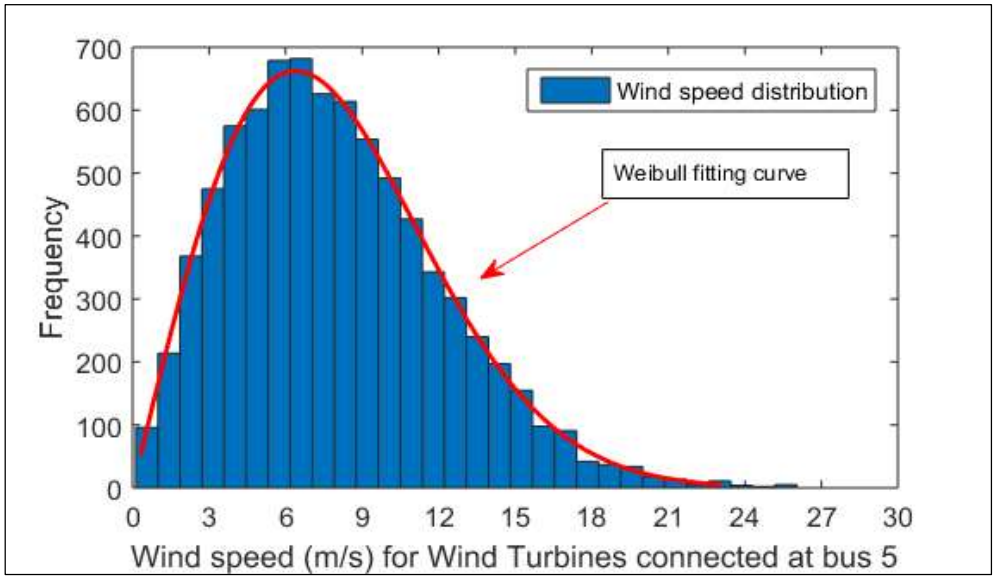

Figure 2. Distribution of wind speed for WTs sources connected at bus 5.

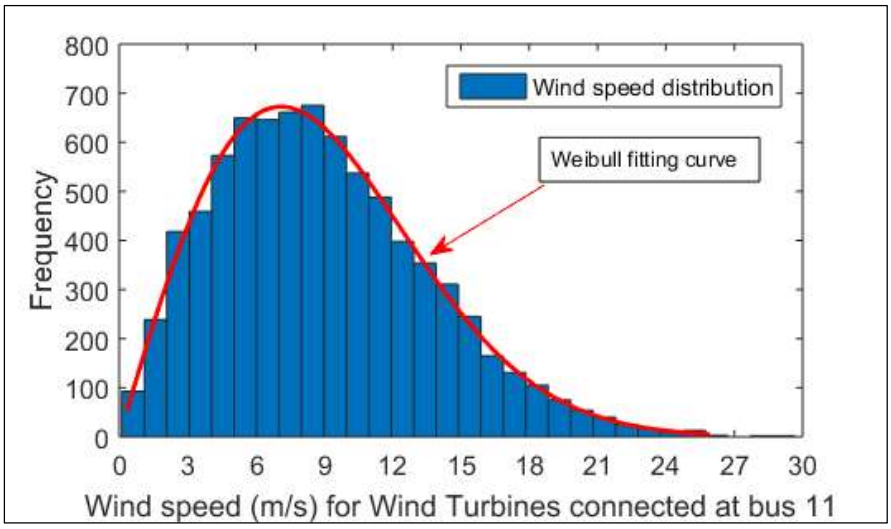

Figure 3. Distribution of wind speed for WTs sources connected at bus 11.

The generated power output of WTs sources relies on wind speed and can be computed in the following manner:

$$P_w(v) = \begin{cases} 0, & for\ \ v < v_{in}\ and\ v < v_{out} \\ P_{wr}, & for\ v_{in} \le v\ \le v_r \\ P_{wr}, & for\ v_r \le v\ \le v_{out} \end{cases} \tag{19}$$

where $v_{in,}$ v_r and v_{out} denote the cut-in, rated, and cut-out wind speeds, respectively.

b) The formulation of stochastic power of solar photovoltaic (SP) source

The power output from the SP source depends on solar irradiance (*G)*, which obeys lognormal PDF [5]. This lognormal PDF is characterized by a mean value (μ) and a standard deviation (σ) and it can be employed to determine the statistical distribution of solar irradiance (σ) using the subsequent equation:

$$f_G(S) = \frac{1}{G\sigma\sqrt{2\pi}} \exp\left\{\frac{-(\ln x - \mu)^2}{2\sigma^2}\right\} \ \text{for}\ \ G\ > 0. \tag{20}$$

The variables associated with lognormal PDF are provided in Table 4, kept the same as cited in the source [5]. Upon execution of 8,000 Monte Carlo simulations, Figure 4 displays both the frequency distribution of solar irradiance and the lognormal fitting curve.

Table 4. Numerical values of cost coefficients and PDF parameters for SP and SHP source.

Bus No. 13	$P_{rated}(MW)$	**lognormal& Gumbel PDF parameters**	**Direct cost coefficient**	**Reserve cost coefficient**	**Penalty cost coefficient**
SP	50	$\mu = 6 \quad \sigma = 0.6$	$h_k = 1.6$	$K_{R-sh} = 3$	$K_{R-sh} = 1.4$
SHP	5	γ_{hp}=15 $\omega^{hp} = 1.2$	$h_l = 1.5$		

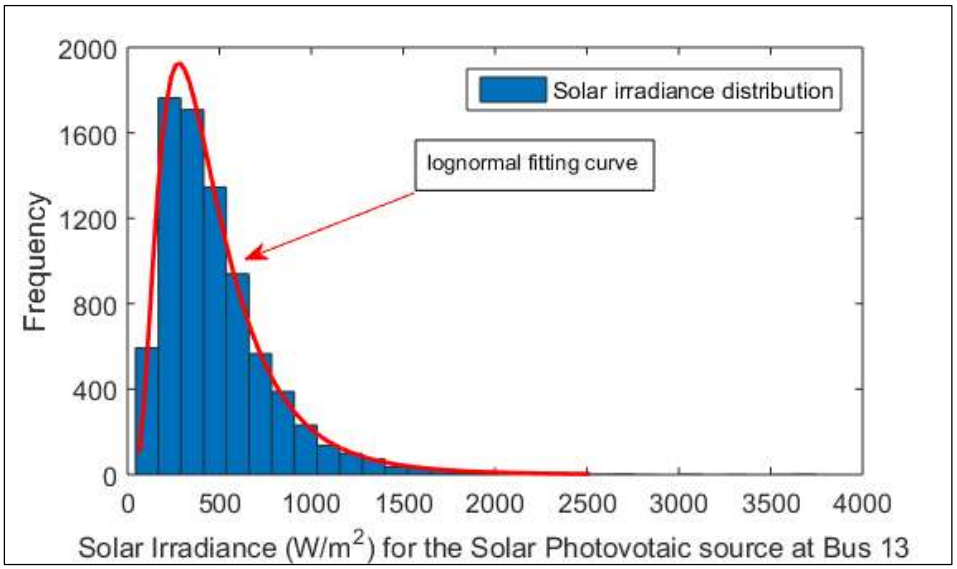

Figure 4. Distribution of solar irradiance for SP source connected at bus 13.

The mathematical representation of the generated power from the SP source, which depends on solar irradiance (G), is presented in Eq (21).

$$P_{SP}(G) = \begin{cases} P_{sr}(\frac{G^2}{G_{std}Rc}) & for\ 0 < G < Rc \\ P_{sr}(\frac{G^2}{G_{std}Rc}) & for\ G \geq Rc. \end{cases} \tag{21}$$

The particular irradiance value is represented by Rc and is set at a value of 120 W/m².

The formulation of stochastic power of small hydropower (SHP) source

In the adapted IEEE 30-bus network, the traditional TG source at bus 13 is substituted with a 50 MW SP and a 5 MW small SHP source. It is widely recognized that the river flow rate conforms to the Gumbel distribution [34]. The probable dissemination of the river flow rate G_{hp}, adhering to the Gumbel distribution $f_{hp}(G_{hp})$ characterized by the location parameter λ^{hp} and scale parameter ω^{hp}, can be formulated as:

$$f_{hp}(G_{hp}) = \frac{1}{\omega^{hp}} \exp\left(\frac{G_{hp} - \gamma_{hp}}{\omega^{hp}}\right) \exp\left[-\exp\left(\frac{G_{hp} - \gamma_{hp}}{\omega^{hp}}\right)\right]. \tag{22}$$

The associated PDF values for these adjustments are detailed in Table 4, with numerous selections made in accordance with a comprehensive investigation cited in Reference [34]. Figures 5–8 depict the real power availability and river flow rate distribution for both SP and SHP sources.

The amount of power generated by a SHP source relies on both the rate of water flow (G_{hp}) and the actual pressure head (h). The output power from SHP can be formalized as follows [34]:

$$P_{hp}(G_{hp}) = \eta^{hp} \delta^{hp} g G_{hp} h \tag{23}$$

where η^{hp} and δ^{hp} denotes the efficiency of the SHP and water density, respectively.

The numerical values involved in the calculation of the SHP source output are kept the same as in reference [34], which are: $\eta^{hp} = 0.85$, $\delta^{hp} = 1000\text{kg/m}^3$, h = 25m, and g = 9.81m/s^2.

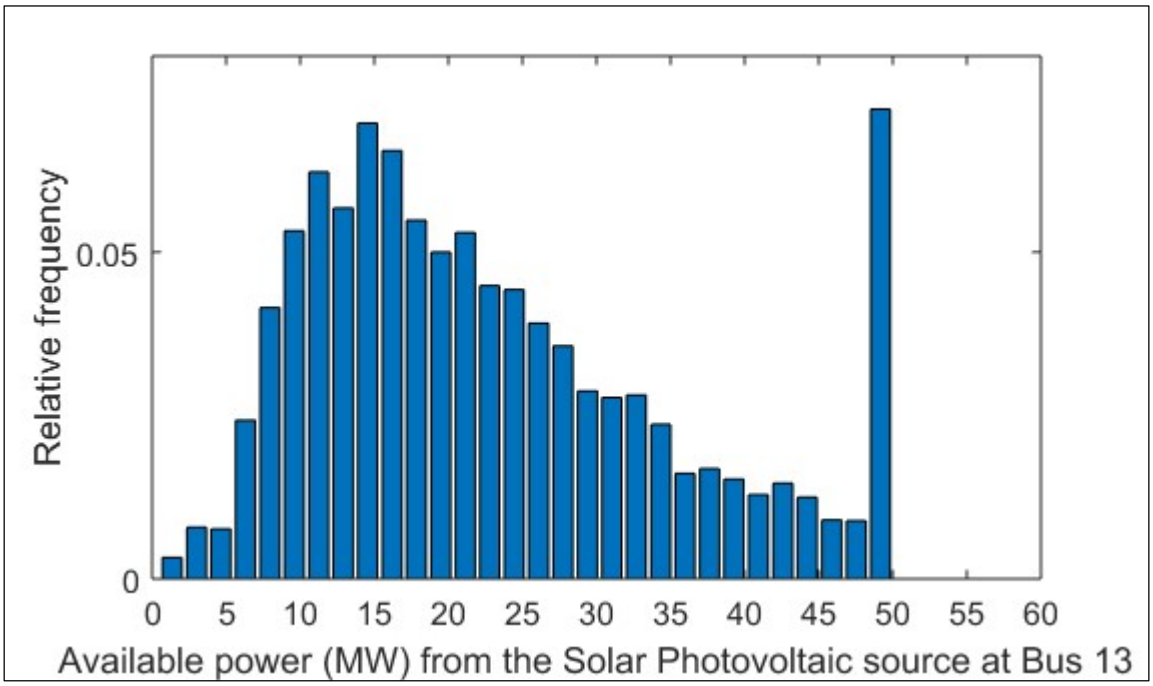

Figure 5. Real power (MW) available from SP source connected at bus 13.

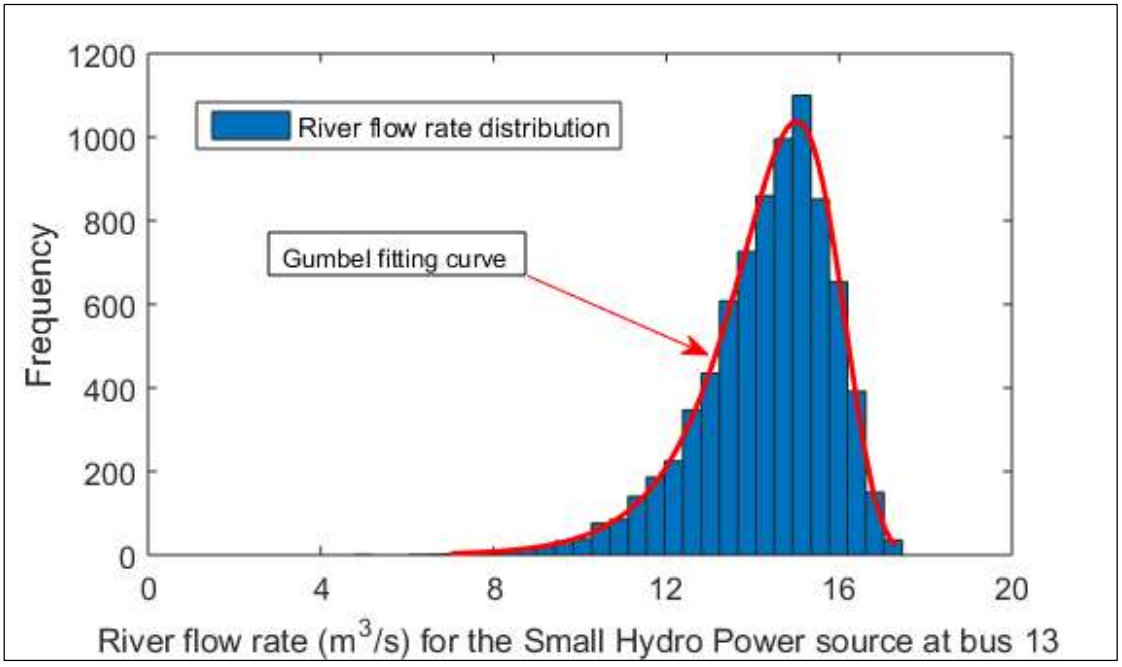

Figure 6. Distribution of river flow rate for SHP source connected at bus 13.

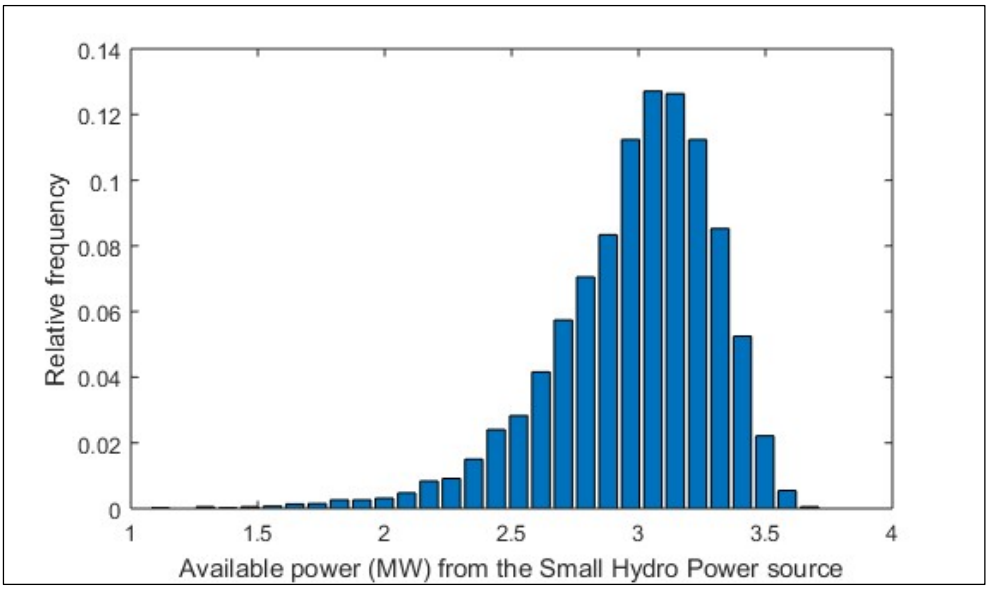

Figure 7. Real power (MW) available from SHP source connected at bus 13.

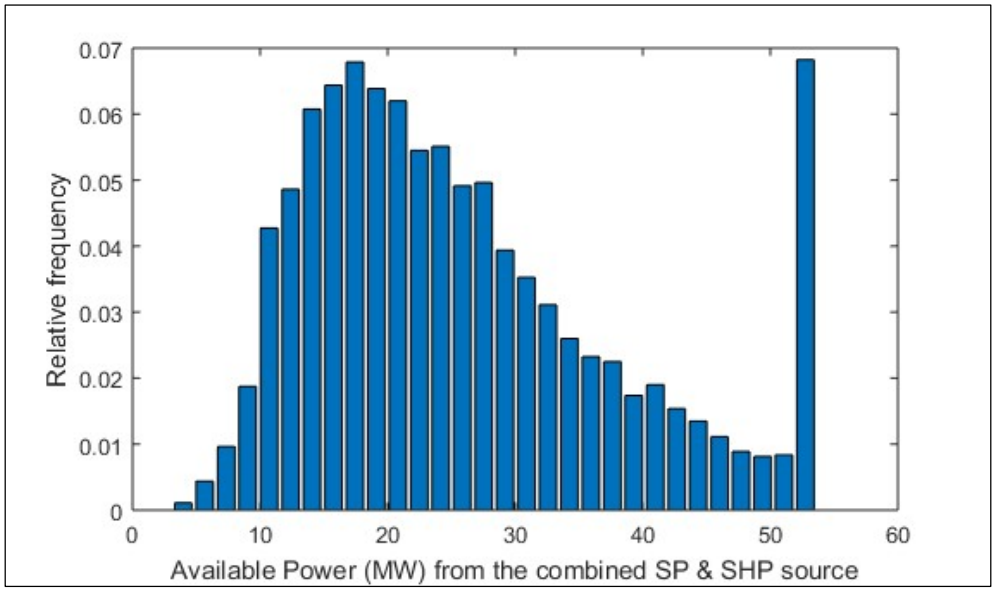

Figure 8. Real power (MW) available from the combined SP and SHP source connected at bus 13.

4. The proposed grey wolf particle swarm optimization (GWPSO) algorithm

In this study, the GWPSO algorithm was employed to optimize the three objective functions discussed earlier. The GWO algorithm replicates the hierarchical hunting and leadership patterns of gray wolves, whereas the PSO algorithm takes inspiration from the collective behaviors exhibited by flocking birds. The GWO algorithm outperforms in exploring the entire exploration area, but exhibits slower convergence and limited local search capability, whereas the PSO algorithm excels in exploitation but can become trapped in local optima [35]. In this study, an algorithm named GWPSO is proposed, which improves GWO's exploration with PSO's exploitation competence to make a collaborative algorithm. The flowchart depicting the chosen GWPSO algorithm is presented in Figure 9.

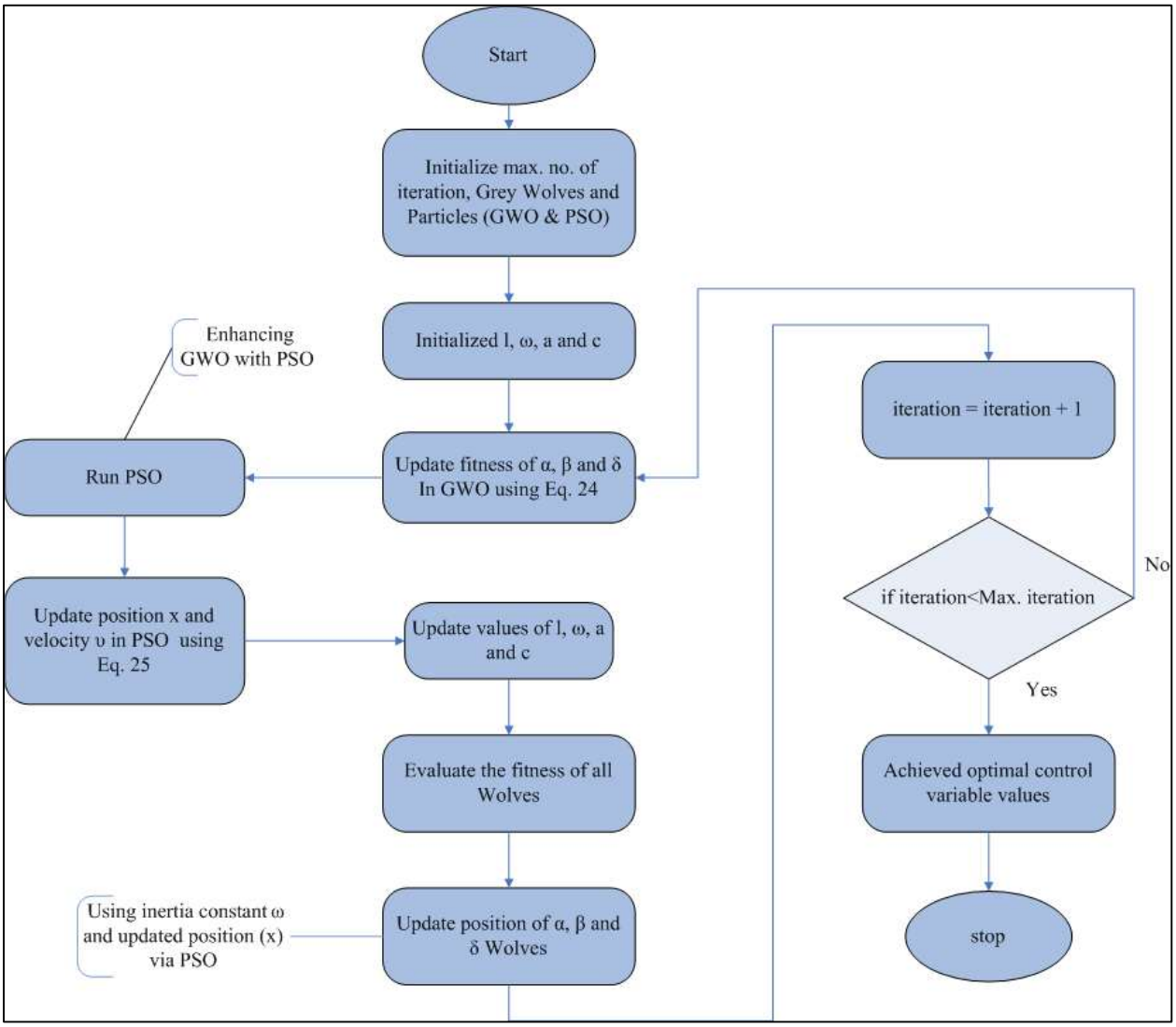

Figure 9. Flowchart of the selected GWPSO algorithm.

In the formulated GWPSO algorithm, the coordinates of alpha (d_α), beta (d_β) and delta (d_δ) within the exploration space are progressively adjusted using the subsequent sequential equations [5]:

$$\begin{aligned} d_\alpha &= \left|c_1.x_\alpha - \omega * x\right| \\ d_\beta &= \left|c_2.x_\beta - \omega * x\right| \\ d_\delta &= \left|c_3.x_\delta - \omega * x\right| \end{aligned}. \tag{24}$$

In the aforementioned expression, the abilities of gray wolves are synchronized within the search region through the use of a momentum constant (c_i) and inertia weight (ω). The modified equations for position (x_i^{k+1}) and (v_i^{k+1}) velocity undergo the following changes [5]:

$$\begin{aligned} x_i^{k+1} &= x_i^k + v_i^{k+1} \\ v_i^{k+1} &= \omega * (v_i^k + c_1 r_1 (x_1 - x_i^k) + c_2 r_2 (x_2 - x_i^k) + c_3 r_3 (x_3 - x_i^k)) \end{aligned}. \tag{25}$$

5. The simulation results and analysis

This study focuses on integrating a SHP source into the modified IEEE 30 bus system, along with integrated WT and SP sources. The main contribution lies in the development of a GWPSO algorithm, aiming to minimize the total generation cost in this hybrid energy system. The optimization of the overall generation cost has been categorized into three scenarios: One without including the valve point effect, one with the valve point effect, and another involving a carbon tax on TGs emissions. Every optimization algorithm is executed five times, for an accumulated sum of 500 iterations in each execution. In each case the results of GWPSO are compared with GWO, PSO and with the previous research as cited in reference [5], where only WTs and SP sources were integrated. In each case, results indicate a decrease in the range of **2.211** to **3.434 $/h** has been observed after incorporating the SHP source into the system. The success of the proposed GWPSO algorithm can be attributed to its effective combination of the exploration capabilities of GWO and the strong convergence abilities of PSO algorithms. The major shortcoming of the proposed algorithm is that its execution time is longer than that of individual algorithms. The study under research provides a solution to the IEEE 30 bus system with integrated GRES while considering static loads. The dynamic nature of load and storage batteries as a backup source to mitigate the uncertain nature of GRES is left for future research work.

5.1 Case 1: Variations in different types of cost as a function of PDF parameters

This scenario examines the interdependencies among reserve cost, penalty cost, direct cost, and total cost for SP and WTs sources in relation to lognormal and Weibull PDF variables, respectively. Maintaining a constant shape parameter (k=2) while varying the scale parameter (c) within the range of 2 to 16. The corresponding cost changes are then observed at fixed scheduled power outputs of 25 MW for WT1 and 20 MW for WT2. These selected power levels represent approximately one third of the overall deployed set up, which aligns with typical practical WT capacity percentages ranging from 30% to 45% [5]. Figures 10 and 11 illustrate the cost curves for WT1 and WT2 sources respectively. Notably, the minimum total cost occurs when the scale parameter (c) is around 9.

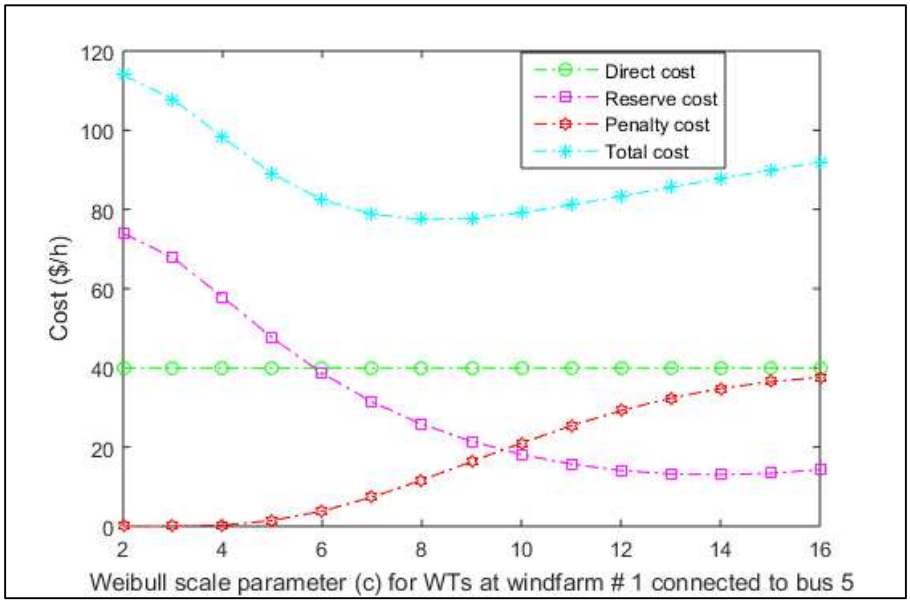

Figure 10. Variations in cost vs scale parameter c (k=2) for WTs connected at bus 5.

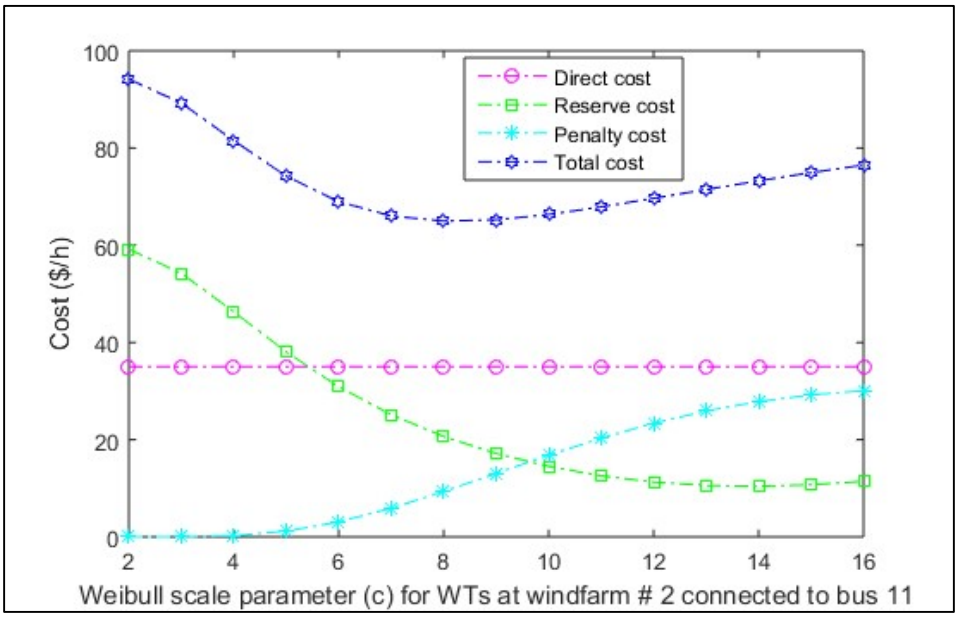

Figure 11. Variations in cost vs scale parameter c (k=2) for WTs connected at bus 11.

Similarly, the SP costs are examined against lognormal mean (μ) spanning from 2 to 7, while maintaining the value of standard deviation σ at 0.6 and a scheduled power output of 20 MW from the SP source. The analysis reveals that the minimum total cost is achieved when the lognormal mean value is set at 6. After μ reaches 6, the penalty and reserve costs converge, but beyond this point, the penalty cost sharply increases, leading to an escalation in total cost. The output power of the SP source is particularly sensitive to the lognormal μ, with higher values of μ requiring greater reserve capacity and vice versa. Figure 12 visualizes the variations in SP cost in relation to the lognormal μ.

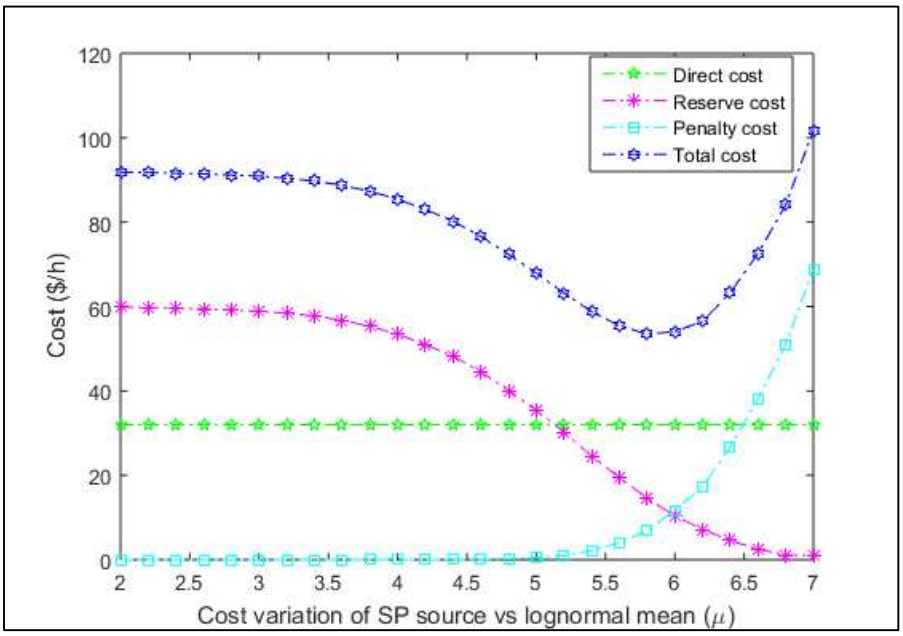

Figure 12. Variations in cost vs lognormal mean μ (σ = 0.6) for SP source connected at bus 13.

5.2 Case 2: Variations in different types of cost as a function of scheduled output power

This scenario examines the impact of varying the planned wind power for two WT sources linked to buses 5 and 11. The scheduled wind power ranges from zero to the WT's rated power has been examined how the reserve cost, penalty cost, direct cost and total cost change accordingly, as illustrated in Figures 13 and 14. The simulation findings indicate that the reserve cost decreases with an increase in the scheduled WT power, indicating an inverse relationship. Conversely, the penalty cost increases with higher scheduled power levels. Interestingly, there exists a direct relationship between the planned wind power and direct cost. The total cost demonstrates an upward trend as the scheduled power increases, as it includes the combination of reserve cost, penalty cost and direct cost elements.

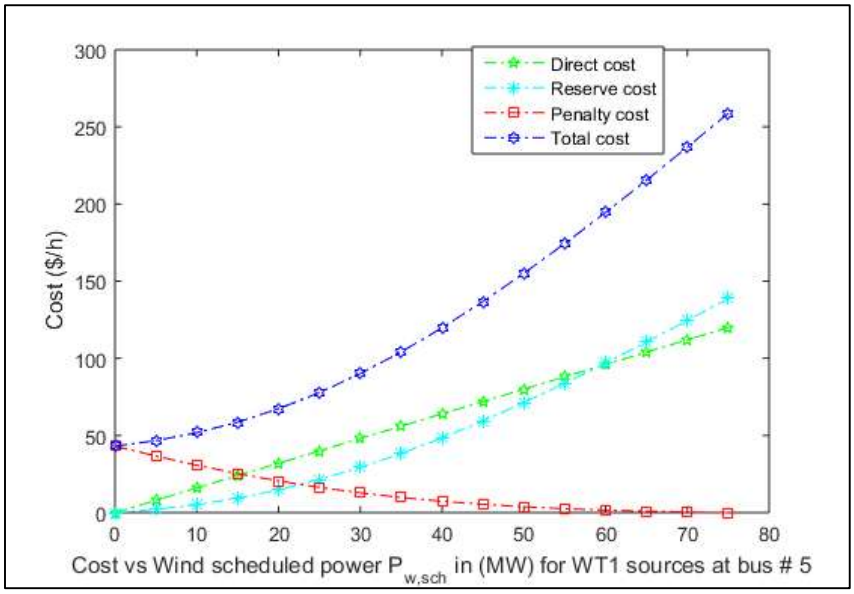

Figure 13. Variations in cost vs schedule power output of WTs sources connected at bus 5.

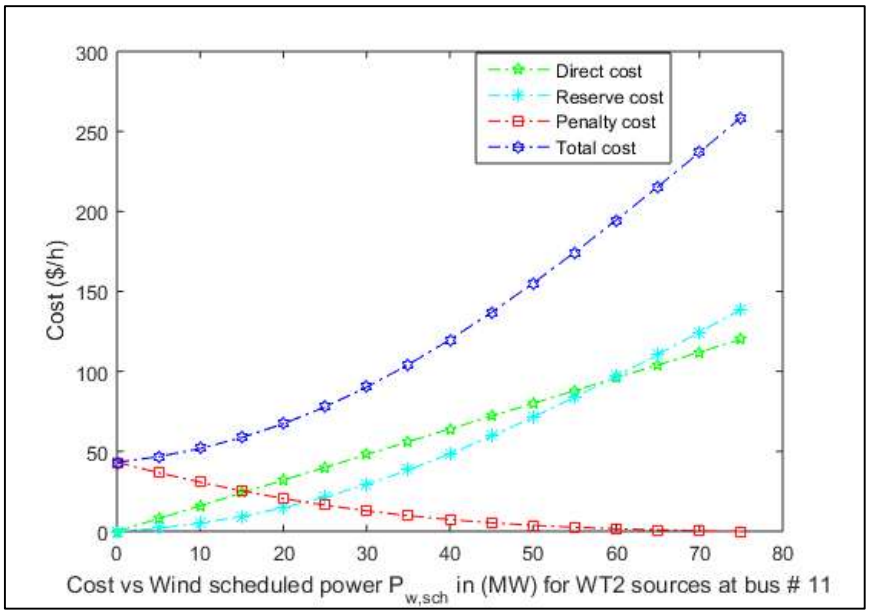

Figure 14. Variations in cost vs schedule power output of WTs sources connected at bus 11.

In a similar manner, the performance of the SP source connected to bus 13 in terms of reserve cost, penalty cost, direct cost and total cost relative to the SP schedule power has been analyzed, as illustrated in Figure 15. The various parameters and cost coefficients can be found in Tables 3 and 4 for reference. Unlike the wind scenario, the total cost for the SP source attains its minimum value at approximately 15 MW.

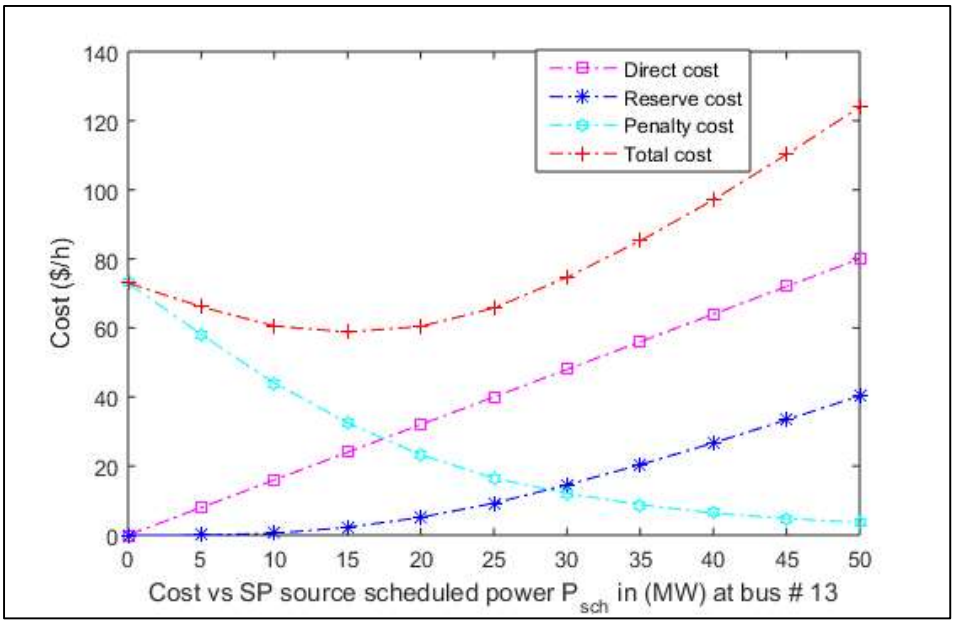

Figure 15. Variations in cost vs schedule power output of a SP source connected at bus 13.

5.3 Case 3: Minimizing the overall generation cost ignoring the valve positioning influence for TGs

In this case, the overall generation cost has been optimized ignoring the valve positioning influence for TGs as formulated in the first objective function in Eq (13). The numerical values of control and constraints parameters obtained from GWO, PSO, and GWPSO, along with the respective values of our previous research work [5], have been considered in Table 5 for the purpose of comparison. The graphs illustrating the convergence trends of GWO, PSO, and the GWPSO algorithms in Figure 16 reveal that the GWPSO approach displays a rapid and consistent curve. The lowest generation cost achieved through GWPSO is 769.302 $/h, which is 3.434 $/h less than that reported in [5], and this difference becomes a significant amount of (3.434×24×365) 30081 $/Y.

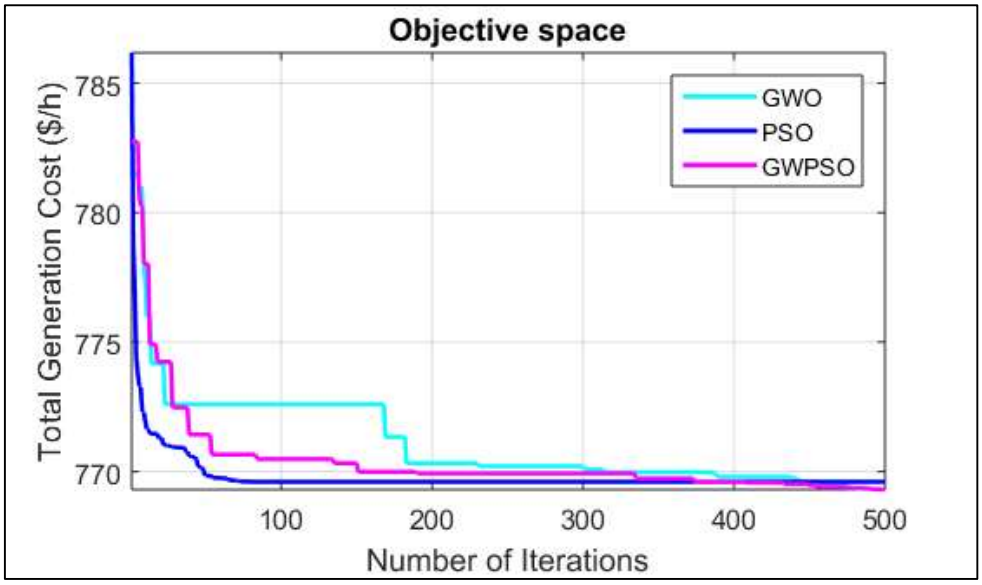

Figure 16. Convergence curves of GWO, PSO and GWPSO algorithms for Case 3.

Table 5. Results from the simulation refer to Case 3.

	parameters	**Min. Value**	**Max. Value**	**GWO**	**PSO**	**GWPSO**	**[5]**
Swing generator	$P_{TG1(MW)}$	50	140	137.711	137.147	136.774	133.046
Control variables	$P_{TG2(MW)}$	20	80	38.575	39.068	39.628	38.418
	$P_{WT5(MW)}$	0	75	39.312	39.809	39.401	39.344
	$P_{TG8(MW)}$	10	35	10.060	10.000	10.000	10.000
	$P_{WT11(MW)}$	0	60	33.860	33.837	33.888	33.257
	$P_{SH13(MW)}$	0	55	29.865	29.426	29.330	35.174*
	$V_{1(p.u.)}$	0.95	1.10	1.10	1.10	1.10	1.10
	$V_{2(p.u.)}$	0.95	1.10	1.09	1.09	1.09	1.090
	$V_{5(p.u.)}$	0.95	1.10	1.07	1.07	1.07	1.068
	$V_{8(p.u.)}$	0.95	1.10	1.08	1.10	1.10	1.098
	$V_{11(p.u)}$	0.95	1.10	1.10	1.10	1.10	1.10
	$V_{13(p.u.)}$	0.95	1.10	1.08	1.09	1.10	1.094
Generator reactive power	$Q_{TG1(MVAr)}$	-20	150	-10.364	-11.665	-17.146	-6.721
	$Q_{TG2(MVAr)}$	-20	60	19.105	19.033	25.064	4.773
	$Q_{WT5(MVAr)}$	-30	35	27.695	25.528	26.544	35.000
	$Q_{TG8(MVAr)}$	-15	40	40.000	40.000	40.000	40.000
	$Q_{WT11(MVAr)}$	-25	30	21.019	19.230	18.643	17.862
	$Q_{SH13(MVAr)}$	-20	25	16.832	21.621	20.507	22.235
Objective functions	Gen cost($/h)	-	-	769.311	769.599	**769.302**	772.736
	P_{loss} (MW)	-	-	5.950	5.887	5.898	5.763
	Emission(t/h)	-	-	2.095	2.022	1.976	1.570
	V.D (p.u.)	-	-	0.891	1.027	1.041	1.047

* $P_{SP\,(}$Max) = 50MW.

5.4 Case 4: Minimizing the total generation cost excluding a carbon tax on emissions from TGs

In this case, the total generation cost has been optimized with consideration of the valve positioning influence for TGs, excluding the incorporation of a carbon tax on TGs emissions as formulated in the second objective function in Eq (14). The numerical values of control and constraints parameters obtained from GWO, PSO, and GWPSO, along with the respective values of our previous research as cited in [5], have been compiled in Table 6 for the purpose of comparison. Figure 17 depicts the convergence curves for the GWO, PSO, and GWPSO algorithms. The achieved minimum generation cost by GWPSO is 778.171 \$/h, which is 2.416 \$/h less than that reported in [5], and this difference becomes a significant amount of (2.416×24×365) 21164 \$/Y.

Table 6. Results from the simulation refer to Case 4.

	parameters	**Min. Value**	**Max. Value**	**GWO**	**PSO**	**GWPSO**	**[5]**
Swing generator	$P_{TG1\ (MW)}$	50	140	135.096	134.908	135.128	135.053
Control variables	$P_{TG2\ (MW)}$	20	80	30.566	30.156	30.106	27.630
	$P_{WT5\ (MW)}$	0	75	44.209	43.782	44.324	43.290
	$P_{TG8\ (MW)}$	10	35	10.010	10.000	10.000	10.000
	$P_{WT11\ (MW)}$	0	60	37.861	37.291	36.974	37.224
	$P_{SH13\ (MW)}$	0	50	31.331	32.761	32.574	35.845*
	$V_{1\ (p.u.)}$	0.95	1.10	1.10	1.10	1.10	1.099
	$V_{2\ (p.u.)}$	0.95	1.10	1.09	1.09	1.09	1.088
	$V_{5\ (p.u.)}$	0.95	1.10	1.07	1.07	1.07	1.072
	$V_{8\ (p.u.)}$	0.95	1.10	1.09	1.09	1.08	1.099
	$V_{11\ (p.u)}$	0.95	1.10	1.10	1.10	1.10	1.099
	$V_{13\ (p.u.)}$	0.95	1.10	30.566	1.09	1.10	1.095
Generator reactive powers	$Q_{TG1(MVAr)}$	-20	150	-4.408	-10.837	14.154	-13.645
	$Q_{TG2(MVAr)}$	-20	60	16.137	17.944	-20.000	22.185
	$Q_{WT5(MVAr)}$	-30	35	20.534	24.911	35.000	25.071
	$Q_{TG8(MVAr)}$	-15	40	40.000	40.000	40.000	40.000
	$Q_{WT11(MVAr)}$	-25	30	20.571	19.288	19.552	20.023
	$Q_{SH13(MVAr)}$	-20	25	20.287	21.425	25.000	19.259
Objective functions	Gen. cost (\$/h)	-	-	778.174	778.255	**778.171**	780.587
	P_{loss} (MW)	-	-	5.505	5.498	5.654	5.532
	Emission (t/h)	-	-	1.782	1.762	1.785	1.778
	V.D (p.u.)	-	-	0.954	1.039	0.976	0.978

* $P_{SP\ (}$Max) = 50MW.

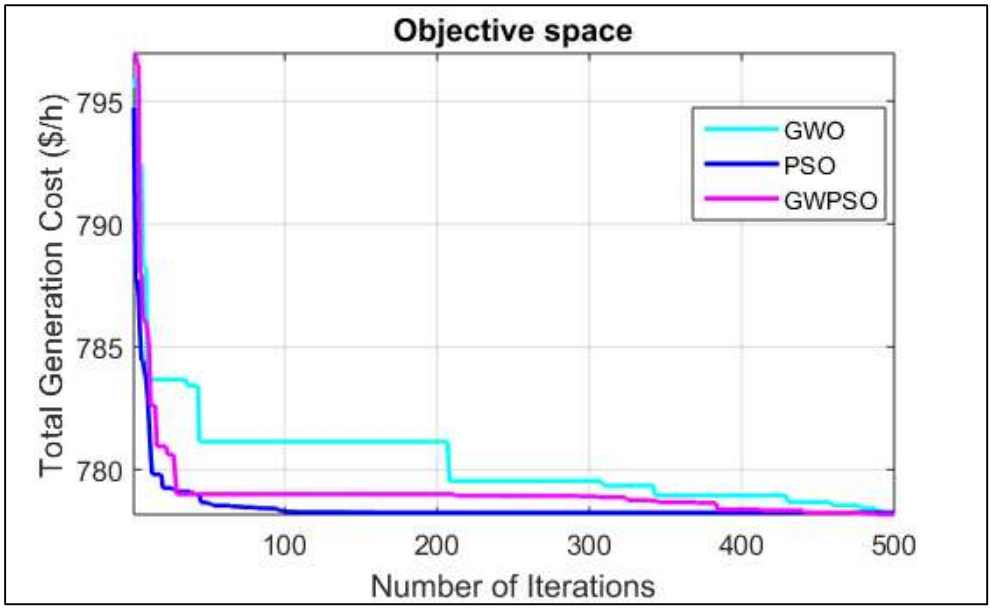

Figure 17. Convergence curves of GWO, PSO and GWPSO algorithms for Case 4.

5.5 Case 5: Minimizing the overall generation cost including a carbon tax applied to emissions from TGs

In this scenario, the total generation cost has been optimized with the inclusion of both the valve positioning influence and a carbon tax applied to emissions from TGs, as formulated in the third objective function in equation 15. The numerical values of control and constraints parameters obtained from GWO, PSO, and GWPSO, along with the respective values of our previous research work [5], have been consolidated in Table 7 for the purpose of comparison. Figure 18 depicts the convergence patterns of the GWO, PSO, and GWPSO algorithms. The achieved minimum generation cost by GWPSO is 807.066 $/h, which is 2.211 $/h less than that reported in [5], and this difference becomes a significant amount of (2.211×24×365) 19368 $/Y. Following the implementation of a carbon tax (20$/ton) on emissions, a reduction of 0.847 ton/h has been observed, this becomes a significant amount of (0.847x24x365) 7420 ton/Y as depicted in Tables 6 and 7.

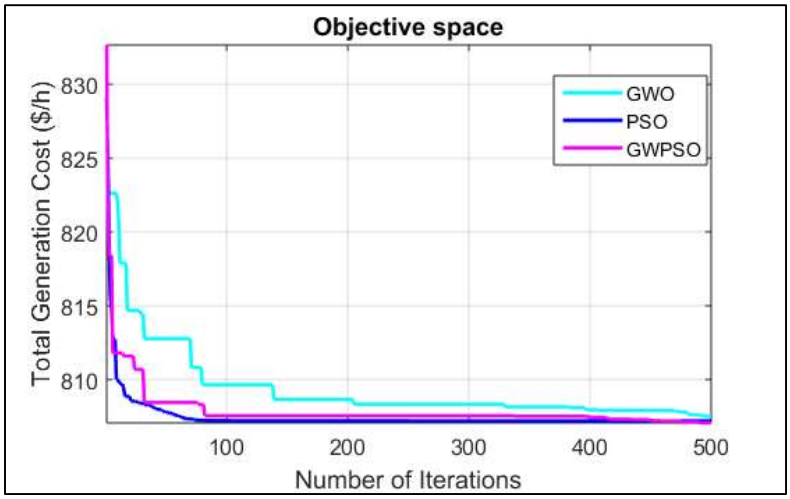

Figure 18. Convergence curves of GWO, PSO and GWPSO algorithms for Case 5.

Table 7. Results from the simulation refer to Case 5.

	parameters	Min. Value	Max. Value	GWO	PSO	GWPSO	[5]
Swing generator	$P_{TG1(MW)}$	50	140	124.521	123.855	124.400	123.956
Control variables	$P_{TG2(MW)}$	20	80	33.995	34.464	33.713	33.605
	$P_{WT5(MW)}$	0	75	47.210	46.492	46.761	46.226
	$P_{TG8(MW)}$	10	35	10.032	39.216	10.002	10.000
	$P_{WT11(MW)}$	0	60	39.427	34.385	39.326	39.033
	$P_{SH13(MW)}$	0	50	33.425	1.10	34.215	35.785*
	$V_{1(p.u.)}$	0.95	1.10	1.10	1.09	1.10	1.100
	$V_{2(p.u.)}$	0.95	1.10	1.09	1.07	1.09	1.090
	$V_{5(p.u.)}$	0.95	1.10	1.07	1.10	1.07	1.071
	$V_{8(p.u.)}$	0.95	1.10	1.08	1.10	1.10	1.088
	$V_{11(p.u)}$	0.95	1.10	1.10	1.09	1.10	1.100
	$V_{13(p.u.)}$	0.95	1.10	1.10	34.464	1.10	1.095
Generator reactive powers	$Q_{TG1(MVAr)}$	-20	150	-18.912	-10.339	-9.453	12.264
	$Q_{TG2(MVAr)}$	-20	60	26.553	16.847	14.816	-20.000
	$Q_{WT5(MVAr)}$	-30	35	22.547	24.578	25.090	35.000
	$Q_{TG8(MVAr)}$	-15	40	40.000	40.000	40.000	40.000
	$Q_{WT11(MVAr)}$	-25	30	18.938	19.103	18.786	19.916
	$Q_{SH13(MVAr)}$	-20	25	22.302	21.124	22.102	24.979
Objective functions	Gen. cost ($/h)	-	-	807.476	807.201	**807.066**	809.277
	P_{loss} (MW)	-	-	5.0406	5.012	5.0130	5.132
	Emission (t/h)	-	-	0.944	0.908	0.938	0.914
	Carbon tax	-	-	18.881	18.160	18.750	18.28
	V.D (p.u.)	-	-	1.074	1.059	1.06418	1.027

* $P_{SP\,(}$Max) = 50MW**.**

6. Conclusions

This study offers a green and economic approach for solving the OPF problem, combining conventional TGs with WTs, SP, and SHP sources by utilizing a GWPSO algorithm. The intermittent nature of WTs, SP, and SHP sources is modeled with Weibull, Lognormal, and Gumbel PDF, respectively. The total generation cost has been optimized while considering the constraints of the system, including equality, inequality, and line capacity constraints. The effectiveness and flexibility of the GWPSO algorithm have been evaluated using a test system that incorporates GRES. The superiority of the GWPSO algorithm has been validated through comparison with the outcomes of the PSO and GWO algorithms. The addition of SHP source along with WTs and SP source has been proven fruitful in the reduction of overall generation cost. The inclusion of a carbon tax led to a decrease in emissions by **7420 tons/Y**, leading to a higher penetration from GRES. The main drawback of the suggested algorithm is its longer execution time compared to individual algorithms. The study focuses on addressing the IEEE 30 bus system with integrated GRES, taking static loads into account. However, the dynamic aspects of load and the utilization of storage batteries as a backup to manage

the uncertainty of GRES are designated for future research. In the future, the GWPSO algorithm will find effective applications in higher bus systems such as IEEE 57 and IEEE 118 bus systems expansions and planning studies.

Use of AI tools declaration

The authors declare that they have not used Artificial Intelligence (AI) tools in the creation of this article.

Acknowledgements

The authors are thankful to the Deanship of Scientific Research at Najran University for funding this work, under the Distinguished Research Program grant code (NU/DRP/SERC/12/7). The authors extend their appreciation to the Deanship of Scientific Research at King Khalid University for funding this work through large groups under grant number RGP2/105/44.

Conflict of interest

The authors declare no conflicts of interest.

References

1. C. P. Anke, D. Möst, The expansion of RES and the EU ETS-valuable addition or conflicting instruments? *Energ. Policy*, **150** (2021), 112125. https://doi.org/10.1016/j.enpol.2020.112125
2. A. Alzahrani, M. A. Hayat, A. Khan, G. Hafeez, F. A. Khan, M. I. Khan, et al., Optimum sizing of stand-alone microgrids: Wind turbine, solar photovoltaic, and energy storage system, *J. Energy Storage*, **73** (2023), 108611. https://doi.org/10.1016/j.est.2023.108611
3. E. Dogan, T. Luni, M. T. Majeed, P. Tzeremes, The nexus between global carbon and renewable energy sources: A step towards sustainability, *J. Clean. Prod.*, **416** (2023), 137927. https://doi.org/10.1016/j.jclepro.2023.137927
4. B. Atems, J. Mette, G. Y. Lin, G. Madraki, Estimating and forecasting the impact of nonrenewable energy prices on US renewable energy consumption, *Energ. Policy*, **173** (2023), 113374. https://doi.org/10.1016/j.enpol.2022.113374
5. M. Riaz, A. Hanif, S. J. Hussain, M. I. Memon, An optimization-based strategy for solving optimal power flow problems in a power system integrated with stochastic solar and wind power energy, *Appl. Sci.*, **11** (2021), 6883. https://doi.org/10.3390/app11156883
6. P. P. Biswas, P. N. Suganthan, G. A. J. Amaratunga, Optimal power flow solutions incorporating stochastic wind and solar power, *Energ. Convers. Manage.*, **148** (2017), 1194–1207. https://doi.org/10.1016/j.enconman.2017.06.071
7. D. S. Kirschen, H. P. V. Meeteren, MW/voltage control in a linear programming based optimal power flow, *IEEE T. Power Syst.*, **3** (1988), 481–489. https://doi.org/10.1109/59.192899
8. M. F. Bedrinana, M. J. Rider, C. A. Castro, *Ill-conditioned optimal power flow solutions and performance of non-linear programming solvers*, 2009 IEEE Bucharest PowerTech, IEEE, 2009. https://doi.org/10.1109/PTC.2009.5282232

9. P. Fortenbacher, T. Demiray, Linear/quadratic programming-based optimal power flow using linear power flow and absolute loss approximations, *Int. J. Elec. Power*, **107** (2019), 680–689. https://doi.org/10.1016/j.ijepes.2018.12.008
10. Y. Guo, S. Sheng, N. Anglani, B. Lehman, *Economically optimal power flow management of grid-connected photovoltaic microgrid based on dynamic programming algorithm and grid I/O strategy for different weather scenarios*, 2019 IEEE Applied Power Electronics Conference and Exposition (APEC), IEEE, 2019. https://doi.org/10.1109/APEC.2019.8722264
11. K. Xie, Y. H. Song, *Dynamic optimal power flow by interior point methods*, IEEE Proceedings-Generation, Transmission and Distribution, **148** (2001), 76–84. https://doi.org/10.1049/ip-gtd:20010026
12. M. S. Osman, M. A. Abo-Sinna, A. A. Mousa, A solution to the optimal power flow using genetic algorithm, *Appl. Math. Comput*., **155** (2004), 391–405. https://doi.org/10.1016/S0096-3003(03)00785-9
13. M. S. Kumari, S. Maheswarapu, Enhanced genetic algorithm based computation technique for multi-objective optimal power flow solution, *Int. J. Elec. Power*, **32** (2010), 736–742. https://doi.org/10.1016/j.ijepes.2010.01.010
14. A. A. A. El-Ela, M. A. Abido, S. R. Spea, Optimal power flow using differential evolution algorithm, *Electric Pow. Syst. Res.,* **80** (2010), 878–885. https://doi.org/10.1016/j.epsr.2009.12.018
15. M. A. Abido, Optimal power flow using particle swarm optimization, *Int. J. Elec. Power*, **24** (2002), 563–571. https://doi.org/10.1016/S0142-0615(01)00067-9
16. I. N. Trivedi, P. Jangir, S. Parmar, N. Jangir, Optimal power flow with voltage stability improvement and loss reduction in power system using Moth-Flame Optimizer, *Neural Comput. Appl.*, **30** (2018), 1889–1904. https://doi.org/10.1007/s00521-016-2794-6
17. I. N Trivedi, P. Jangir, N. Jangir, S. Parmar, *Voltage stability enhancement and voltage deviation minimization using multi-verse optimizer algorithm*, 2016 International conference on circuit, power and computing technologies (ICCPCT), IEEE, 2016. https://doi.org/10.1109/ICCPCT.2016.7530136
18. M. Al-Attar, Y. S. Mohamed, A. A. M. El-Gaafary, A. M. Hemeida, Optimal power flow using moth swarm algorithm, *Electr. Pow. Syst. Res.*, **142** (2017), 190–206. https://doi.org/10.1016/j.epsr.2016.09.025
19. B. Bentouati, C. Saliha, R. A. El-Sehiemy, G. G. Wang, Elephant herding optimization for solving non-convex optimal power flow problem, *J. Electr. Electron. Eng.*, **10** (2017), 31.
20. S. Duman, U. Guvenc, Y. Sönmez, N. Yörükeren, Optimal power flow using gravitational search algorithm, *Energ. Convers. Manage.*, **59** (2012), 86–95. https://doi.org/10.1016/j.enconman.2012.02.024
21. M. H. Nadimi-Shahraki, S. Taghian, S. Mirjalili, L. Abualigah, Ewoa-opf: Effective whale optimization algorithm to solve optimal power flow problem, *Electronics*, **10** (2021), 2975. https://doi.org/10.3390/electronics10232975
22. M. Siavash, C. Pfeifer, A. Rahiminejad, B. Vahidi, *An application of grey wolf optimizer for optimal power flow of wind integrated power systems,* 18th International Scientific Conference on Electric Power Engineering (EPE), IEEE, 2017. https://doi.org/10.1109/EPE.2017.7967230
23. O. D. Garzon-Rivera, J. Ocampo, L. Grisales-Norea, O. Montoya, J. J. Rojas-Montano, Optimal power flow in Direct Current Networks using the antlion optimizer, *Stat. Optim. Inform. Comput.*, **8** (2020), 846–857. https://doi.org/10.19139/soic-2310-5070-1022
24. T. Jumani, M. Mustafa, M. Rasid, N. Mirjat, M. Baloch, S. Salisu, Optimal power flow controller for grid-connected microgrids using grasshopper optimization algorithm, *Electronics*, **8** (2019), 111. https://doi.org/10.3390/electronics8010111

25. S. Khunkitti, A. Siritaratiwat, S. Premrudeepreechacharn, R. Chatthaworn, N. Watson, A hybrid DA-PSO optimization algorithm for multiobjective optimal power flow problems, *Energies*, **11** (2018), 2270. https://doi.org/10.3390/en11092270
26. J. Radosavljevic, D. Klimenta, M. Jevtic, N. Arsic, Optimal power flow using a hybrid optimization algorithm of particle swarm optimization and gravitational search algorithm, *Electr. Pow. Compo. Sys.*, **43** (2015), 1958–1970. https://doi.org/10.1080/15325008.2015.1061620
27. S. Birogul, Hybrid harris hawk optimization based on differential evolution (HHODE) algorithm for optimal power flow problem, *IEEE Access*, **7** (2019), 184468–184488. https://doi.org/10.1109/ACCESS.2019.2958279
28. B. Venkateswararao, D. Ramesh, F. Pedro, G. Márquez, Hybrid approach with combining cuckoo-search and grey-wolf optimizer for solving optimal power flow problems, *J. Electr. Eng. Technol.*, **18** (2023), 1637–1653. https://doi.org/10.1007/s42835-022-01301-1
29. M. Soroush, M. Shahbakhti, J. Sarda, K. Pandya, K. Y. Lee, Hybrid cross entropy—cuckoo search algorithm for solving optimal power flow with renewable generators and controllable loads, *Optim.Contr. Appl. Met.*, **44** (2023), 508–532. https://doi.org/10.1002/oca.2974
30. M. Riaz, A. Hanif, H. Masood, M. A. Khan, An optimal power flow solution of a system integrated with renewable sources using a hybrid optimizer, *Sustainability*, **13** (2021), 13382. https://doi.org/10.3390/su132313382
31. A. M. Shaheen, R. A. El-Sehiemy, H. M. Hasanien, A. Ginidi, An enhanced optimizer of social network search for multi-dimension optimal power flow in electrical power grids, *Int. J. Elec. Power*, **155** (2024), 109572. https://doi.org/10.1016/j.ijepes.2023.109572
32. A. Shaheen, A. Ginidi, R. El-Sehiemy, A. Elsayed, E. Elattar, H. T. Dorrah, Developed Gorilla troops technique for optimal power flow problem in electrical power systems, *Mathematics*, **10** (2022), 1636. https://doi.org/10.3390/math10101636
33. E. Delarue, V. D. B. Kenneth, Carbon mitigation in the electric power sector under cap-and-trade and renewables policies, *Energ. Policy*, **92** (2016), 34–44. https://doi.org/10.1016/j.enpol.2016.01.028
34. P. P. Biswas, P. N. Suganthan, B. Y. Qu, G. A. J. Amaratunga, Multiobjective economic-environmental power dispatch with stochastic wind-solar-small hydro power, *Energy*, **150** (2018), 1039–1057. https://doi.org/10.1016/j.energy.2018.03.002
35. S. Narinder, S. B. Singh, Hybrid algorithm of particle swarm optimization and grey wolf optimizer for improving convergence performance, *J. Appl. Math.*, **2017** (2017). https://doi.org/10.1155/2017/2030489

AIMS Press